SUPERCONDUCTORS, METALLURGY OF DUCTILE ALLOYS

The most widely used superconducting materials are based on Nb–Ti alloys with Ti contents ranging from 46 wt. % to 50 wt. % Ti. These alloys of Nb and Ti have both high strength and ductility and can be processed to achieve high critical current densities that make them ideal candidates for magnets and applications. Nb–Ti-based superconductors are commercially produced in long uniform lengths and cost significantly less to produce than other superconductors. The main drawbacks of this material are a low critical temperature, typically requiring cooling by liquid helium, and a low upper critical field which limits the applied field at which they can be used to below 12 T.

Although several other ductile superconductors have been investigated (most importantly niobium–zirconium), the niobium–titanium alloy system has been the only ductile superconductor in use since the mid-1960s. The vast majority of all superconducting magnets have been constructed from a small Nb–Ti alloy range of 46 wt. % Ti to 50 wt. % Ti (62 at. % Ti to 66 at. % Ti), with most of the superconductor used being 47 wt. % Ti (63 at. % Ti). It is the strength, ductility, critical current density, and relatively low cost of this material that makes it stand out as a commercial superconductor. The critical temperature, T_c, and upper critical field, H_{c2}, of these Nb–Ti alloys are unexceptional ($T_c \sim 9.3$ K, H_{c2} (4.2 K) ~ 11 T, H_{c2} (2 K) ~ 14 T), but their very high critical current densities ($\sim$3000 A/mm^2 at 5 T, 4.2 K) make them the ideal choice for applications in magnetic fields up to 9 T at 4.2 K (liquid helium coolant) and 12 T at 1.9 K (superfluid liquid helium coolant). The primary applications of Nb–Ti-based magnets are magnetic resonance imaging (*MRI*), nuclear magnetic resonance (*NMR*), particle accelerators, magnetic confinement for fusion reactors, ore separators, electrical power conditioners, and superconducting magnetic energy storage (*SMES*). Replacing some Nb with 15 wt. % Ta to 25 wt. % Ta further extends the upper critical field when cooled with superfluid liquid helium but has yet to achieve significantly higher critical current densities. This article will concentrate on Nb–47 wt. % Ti and similar alloys because of their complete dominance as ductile superconductors. Collings (1, 2) has compiled extensive reviews of the properties and applications of ductile Ti-based superconductors and has covered the history of their development up to 1983 in an earlier volume (3).

Almost all Nb–Ti strands are manufactured as a composite of Nb–Ti filaments in a Cu (or occasionally Cu–Ni or Al) matrix. The number of filaments can vary from 50 to 5000, and their diameters can vary from 5 μm to 50 μm. The Cu matrix typically represents 50% to 70% of the strand volume and provides the composite with thermal and electrical stability. Subdividing the filaments provides adiabatic flux-jump stability and allows greater cold work to be applied to the strand, which is beneficial in achieving high critical currents. Commercial scale composites are manufactured on a scale of $\sim$200 kg billets, and the resulting wire lengths can exceed 10 km at final size without breakage.

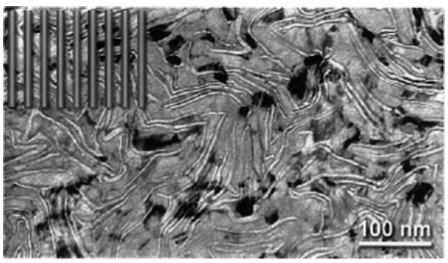

Figure 1. A transmission electron microscope image of the microstructure of a Nb–47 wt. % Ti superconductor in transverse cross section reveals a densely folded array of second phase pins which are 1 nm to 4 nm in thickness. For comparison a schematic illustration of the fluxoid diameter (10 nm) and spacing (22 nm) at 5 T and 4.2 K is superimposed on the top left-hand corner.

In type II superconductors, such as Nb–Ti, high critical current densities in magnetic fields are only possible if fluxoid motion is inhibited. In Nb–Ti, strong fluxoid pinning is made possible by the creation of a finely dispersed nanometer scale nonsuperconducting that closely matches the fluxoid spacing. The method of creating that pinning microstructure distinguishes the two basic methods of producing Nb–Ti strand. Figure 1 shows such a microstructure achieved by heat-treating the strand during processing to produce Ti-rich α-Ti which fold into a densely packed array of sheets when the Nb–Ti wire is drawn to final size. The α-Ti sheets are typically 1 nm to 4 nm thick with a separation of 5 nm to 20 nm. The folding of the microstructure during wire drawing is a result of the limited deformation orientations available in the body-centered cubic (*BCC*), crystal structure of the Nb–Ti grains. Almost all commercial Nb–Ti strands are fabricated using precipitation heat treatment and are termed "conventionally processed" in order to distinguish them from the second and newer method of Nb–Ti production called Artificial Pinning Center (*APC*). In the APC process the pinning microstructure is engineered by mechanically assembling rods or sheets of the component materials at a size large. Extrusion and wire drawing reduces the assembled array to the final nanometer dimensions. Like the conventionally processed strand, the deformation of the engineered microstructure is dominated by the folding of the Nb–Ti matrix grains, and the resulting APC microstructures are very similar in appearance to those produced by conventional processing. The APC approach allows a large degree of freedom in the selection of matrix and pinning materials as well as their ratios and physical distribution. Consequently, APC strands outperform conventionally processed strands in fields up to 5 T and promise greater performance at higher fields. The additional cost associated with assembling the pinning array and reducing it to nanometer scale has limited its commercial application.

THE NB–TI ALLOY SYSTEM

Stable Phases

The atomic volume difference between Ti and Nb is only about 2%, resulting in a β-isomorphous system where the

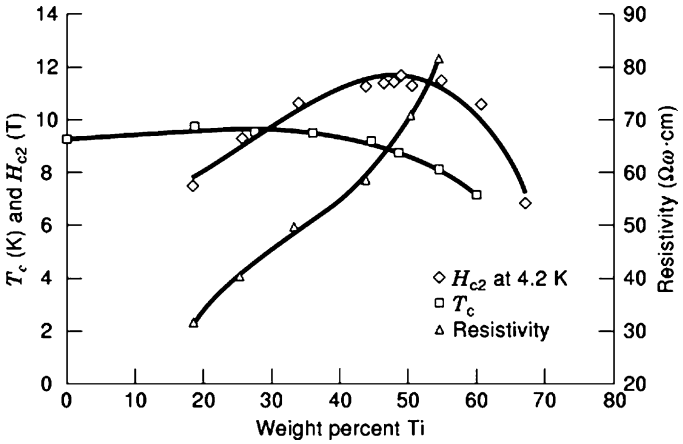

Figure 2. The variation in H_{c2} at 4.2 K (4), T_c (5) and resistivity (6) with composition for single-phase Nb–Ti. H_{c2} is defined as the linear extrapolation of the high-field pinning force (F_p) to zero.

β phase has a BCC structure with a lattice parameter of approximately 0.3285 nm. Figure 2 shows the variation in H_{c2} at 4.2 K (4), T_c (5) and resistivity, ρ_n (6) with composition for single-phase β-Nb–Ti. The upper critical field peaks sharply in the range of 40 wt. % Ti to 50 wt. % Ti with a maximum value of 11.5 T at 44 wt. % Ti. The critical temperature drops continuously over this range with increasing Ti content. The only other stable phase in this system is the Ti-rich α phase which has a hexagonal close-packed (*HCP*) structure and a composition of 1 at. % Nb to 2 at. % Nb. The low Nb content of the α-Ti phase suggests that α-Ti precipitates should have a low T_c (approaching the 0.39 K T_c of pure Ti) and should be nonsuperconducting under practical operating conditions. The beneficial role of precipitating the normal-phase α-Ti precipitates was first shown by Pfeiffer and Hillman in 1968 (7). The alpha phase is only stable below 882°C (at atmospheric pressure); and for the alloy composition range of interest, α-Ti is only stable below 570° to 600°C. In Figure 3 the widely used high-temperature phase boundaries of Hansen et al. (8) are combined with the calculated low temperature boundaries of Kaufman and Bernstein (9) modified by Moffat and Kattner (10) to provide a composite equilibrium phase diagram that generally reflects production experience. The use of the calculated low-temperature phase boundaries is a result of the difficulty of achieving equilibrium at the low temperatures (compared to the melting point) at which the β to $\alpha + \beta$ transformation occurs in Nb–Ti. The interdiffusion rate in β-Nb–Ti decreases exponentially with decreasing Ti content, and it was calculated in 10 that at 500°C it would take 10 years to reach the same condition in a 30 at. % Ti alloy that it would take in 3 s in an 80 at. % Ti alloy. The slow diffusion rates mean that in the composition range for superconducting application the single β phase can be retained even with relatively slow quenching from above $\beta/\alpha + \beta$ boundary (600° to 650°C). The shape and position of the $\beta/\alpha + \beta$ boundary is important because it determines the maximum volume of α-Ti precipitate that can be formed for a given heat treatment temperature and alloy composition. The calculated boundary indicates that both increasing the Ti content and decreasing the heat treatment temperature should increase the maximum volume of precipitate that can be produced.

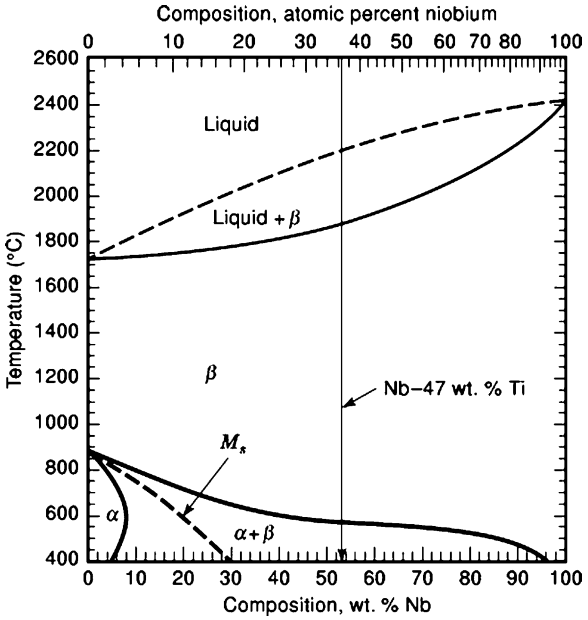

Figure 3. A hybrid equilibrium phase diagram for Nb–Ti combining the experimentally determined high-temperature phase boundaries of Hansen et al. (8) with the calculated low-temperature phase boundaries of Kaufman and Bernstein (9) modified by Moffat and Kattner (10). Also shown is the martensite transformation curve (M_s) of Moffat and Larbalestier (11).

Metastable Phases

There are three metastable phases of importance: two martensite (α' and α'') and an ω phase. The α' martensite is HCP with lattice parameters identical to α-Ti, and it forms in alloys up 7 at. % niobium. The orthorhombic α'' is transitional between the HCP α' and the BCC β phase, and it forms at higher Nb concentrations. The martensite transformation boundary of Moffat and Larbalestier (11) is shown in Fig. 3 and shows that the most commonly used Nb–Ti alloys are outside the range of the martensite transformation. The ω phase has a hexagonal crystal structure ($c/a = 0.613$). It can be formed athermally in the alloy range 86 at. % Ti to 70 at. % Ti by quenching from the β-phase region, or it can be formed by aging in the temperature range of 100° to 500°C. The ω phase is typically observed as small

ellipsoids roughly 5 nm to 10 nm in their longest dimension. In cold-worked and heat-treated Nb–Ti strands, they can grow to 50 nm in diameter. All the metastable phases can be transformed to single-phase β-Nb–Ti or two-phase $\alpha + \beta$ microstructures by heating long enough in the β or $\alpha + \beta$ phase fields, respectively.

Cold-Worked Microstructures

In order to achieve high critical current densities a fine and homogeneous dispersion of flux pinning material must be introduced that is of sufficient volume for significant pinning but does not deleteriously affect the other H_{c2} or T_c. The process by which the first high critical current density microstructures were achieved was arrived at empirically before the resulting microstructures were characterized (12). The processing involved a high cold-work strain followed by three or more heat treatments in the $\alpha + \beta$ phase range, each separated by additional cold work with the final heat treatment being followed by another large cold-work strain. An understanding of the microstructural development was key, however, to the further optimization of Nb–Ti and the reproducible production of high critical current strand. Initial observation of the microstructure was hindered by the difficulty in preparing transverse cross sections of micron-sized filaments suitable for examination by transmission electron microscopy (*TEM*). Once techniques had been developed to prepare the TEM specimens, it became clear that folded sheets of α-Ti precipitates were the dominant microstructural features of the final strand (see Ref. 13). Systematic analysis of the production process (as in Ref. 14) revealed that the high prestrain heat treatments produced α-Ti precipitates only at the intersections of grain boundaries. The location of precipitation at the grain boundary triple points meant that the precipitation was homogeneously distributed if alloy composition and grain size were uniform. The grain boundary triple-point α-Ti was also sufficiently ductile that it could be drawn down to the nanometer scale with breaking up or causing the strand itself to become difficult to draw. This contrasted with the other commonly observed α-Ti precipitate morphology, Widmanstätten α-Ti, which formed in densely packed rafts in the interior of grains and resulted in a great increase in the filament hardness. The next section reviews each step of the process in more detail.

THE CONVENTIONAL PROCESS

Alloy Fabrication

A high-purity fine-grained Nb–Ti alloy with chemical homogeneity over both a large and small microstructural scale is an essential starting point to the production of Nb–Ti strands. The large liquid–solid phase separation shown in the phase diagram (Fig. 3), along with the high melting point of the Nb, makes it particularly difficult and expensive to produce a high-quality Nb–Ti alloy suitable for superconductor application. The main driving force for high homogeneity is the key role that precipitate quantity and morphology play in determining critical current density, both of which are highly sensitive to composition. The development of a high-homogeneity Nb–Ti alloy was a crucial step in the advance toward high critical current Nb–Ti (see Ref. 15). The desired properties of the initial alloy billet are as follows:

1. The correct overall alloy composition to optimize H_{c2}, T_c and precipitation for pinning. The acceptable range is Nb–46-wt. % Ti to Nb–48 wt. % Ti.
2. Uniform composition over the entire billet to ensure optimum physical and mechanical properties over the entire filament.
3. Chemical homogeneity on a microstructural level in order to ensure uniform precipitation of the correct morphology (typically $\pm$ 1.5 wt. % Ti).
4. Low and controlled levels of impurity elements in order to ensure predictable superconducting and mechanical properties.
5. Elimination of hard particles (typically Nb-rich) because any particle that does not co-reduce with the alloy can result in filament drawing instability and ultimately strand breakage. The exterior of the final Nb–Ti rod must also be free of hard particles and must be smooth enough that it does not easily pick up particles during subsequent handling.
6. A fine (typically ASTM grain size 6 or smaller) and uniform grain size as it controls the distribution of precipitate nucleation sites. A fine grain size also improves diffusion barrier uniformity. Where high critical current is less important, a larger grain size has been used increase ductility.
7. Low hardness (typically a Vickers hardness number of 170 or less) to ease co-deformation with softer stabilizer material.

The Nb–Ti alloy is prepared from high-purity Nb and Ti by consumable electrode vacuum-arc melting (where the electrodes are composites of Nb and Ti) and by electron-beam or plasma-arc melting. It is usually necessary to remelt the ingot two or three times in order to achieve the necessary chemical homogeneity. Primarily produced for the aviation industry, the high-purity source Ti is reduced from $TiCl_4$ by Mg (the Kroll process). High-purity Nb is refined from lower-purity Nb by two or three electron-beam remelts. The lower-purity Nb source itself is extracted from niobite–tantalite (Nb_2O_5 and Ta_2O_5) or pyrochlore (0.25% to 3% Nb_2O_5) ores by way of an intermediate ferroniobium alloy which is used on a relatively large scale for steel production. Table 1 lists the typical allowable ranges for impurities, typified by specifications for the superconducting supercollider. The small level of allowable Ta has a historical origin, and it is unlikely that additions of less than 1.5 wt. % Ta will have a significant impact on superconducting or mechanical properties. Increasing the level of Fe from 200 μL/L (the specification of the superconducting supercollider as found in Ref. 16) to 500 μL/L (μL/L is equivalent to the more commonly used ppm) actually has a beneficial effect as shown in Ref. 17.

The chemical inhomogeneities that may be observed in the alloy at this stage in production can be divided into two types based on size: macroinhomogeneities (those visible to

Table 1. Typical Nb–Ti Impurity Limits Based on Superconducting Supercollider Specifications

Impurity Element	Upper Limit (μL/L)	Impurity Element	Upper Limit (μL/L)
Ta	2500	Cu	100
O	1000	Ni	100
C	200	Si	100
Fe	200	Cr	60
N	150	H	35
Al	100		

the eye) and microinhomogeneities (those requiring identification using microscopes). The most common macroinhomogeneities are Ti-rich "freckles" and hard Nb-rich particles. The Ti-rich freckles are so called from their appearance in ingot cross sections and are a result of Lorentz and buoyancy-driven flow of Ti-rich material between dendrites (see Ref. 18). Control of radial heat transfer and fluid flow in the melt pool eliminates the occurrence of freckles. Because of their relatively small size (typically 1 mm to 2 mm in diameter), compositional deviation (Ti-rich by 8 wt. % Ti to 10 wt. % Ti), and ductility, freckles are not in themselves particularly deleterious to strand production. The importance of the presence or rather the absence of Ti-rich freckles is as an indicator of good melt control. Ti-rich freckles are readily identified from flash radiographs of ingot cross sections. If flash radiography indicates that an ingot cross section is freckle-free, it is likely that smaller-scale microinhomogeneities, which are more difficult and expensive to quantify, have been kept to a minimum. A more serious macroinhomogeneity is the presence of hard Nb-rich particles which result in strand breakage failures (see Ref. 19). Nb-rich regions are a result of the high freezing point of Nb and can be eliminated by good process control and remelting. The Nb-rich particles were the cause of many early strand failures but are rarely seen in modern production.

Microchemical inhomogeneity in the cast ingots of Nb–Ti is inevitable because of the coring produced by the large liquid–solid phase separation. The microhomogeneity level can be qualitatively revealed by metallography using a composition-sensitive etch as shown in Fig. 4. In this example of a high-homogeneity-grade alloy, the microchemical variation is $\pm$ 1 wt. % Ti and has a wavelength of 100 μm to 200 μm. Commercial Nb–Ti alloys have microchemical variations of $\pm$ 1 wt. % Ti to $\pm$ 4 wt. % Ti, with higher-homogeneity alloys costing more. Where high critical current density is less important, reduced microhomogeneity can be acceptable in order to reduce cost but not to an extent that will reduce strand yield by causing drawability problems during subsequent processing.

The diameter of the initial cast Nb–Ti ingot ranges from 200 mm to 600 mm, and this is typically reduced to 150 mm by hot forging before being fully annealed in the single-phase β region (approximately 2 h at 870°C). Extended anneals can be used to reduce microchemical inhomogeneity but will increase the grain size and consequently reduce the density of precipitate nucleation sites.

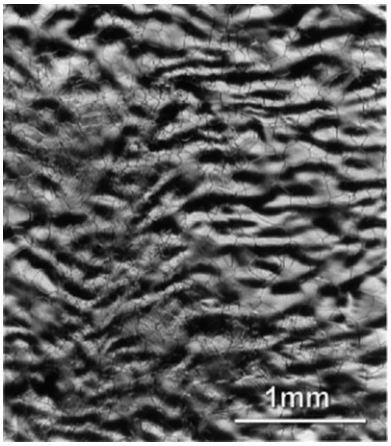

Figure 4. Microchemical inhomogeneity in an Nb–Ti alloy can be revealed using a composition-sensitive etch, as in this example of an high-homogeneity Fe-doped Nb–46 wt. % Ti alloy produced by Teledyne Wah Chang.

Composite Assembly

Stabilizer. All superconducting strands are fabricated as a combination of one or more continuous filaments of superconductor within a high electrical and thermal conductivity matrix. The matrix material provides electrical and thermal stability and protection from burnout if the superconducting device reverts to the normal state ("quenches"). High-purity Cu is most commonly used because it has good electrical and thermal conductivity (a resistivity of 0.42 nΩ·m and a thermal conductivity of 260 W/m·K at 6 T, 4.2 K), a high heat capacity, and good strength at both low temperature and during processing and it combines and processes well as a composite with Nb–Ti. A Cu–Ni stabilizer is used for alternating-current (*ac*) applications where a high-resistivity matrix is required to reduce eddy current loss in the matrix and coupling between the submicron filaments (e.g., Refs. 20 and 21. Where high transverse resistivity is not required, Mn additions to Cu can be used to suppress the proximity coupling of filaments (22). Combinations of high-purity Cu and Cu–Ni or Cu–Mn can be used within the same composite because the alloy stabilizer is only required between filaments. High-purity aluminum has a greater in-field thermal conductivity and electrical conductivity as well as a lower heat capacity, a lower density, and greater radiation resistance than Cu. Despite these considerable advantages, Al is rarely used as a sta-

bilizer because it is extremely difficult to coprocess with Nb–Ti. Furthermore, conventional processing requires the use of precipitation heat treatments that further soften the Al with respect to the Nb–Ti. The use of APC processing avoids the need for precipitation heat treatment and has been used to fabricate Al-stabilized strand with 15 vol. % of Al (23). Additional stabilizer can be added after or late in the fabrication process by external application, by soldering the strand into a channel machined in the external stabilizer, coextruding the strand inside the external stabilizer, or other cladding techniques (24). These methods of applying external stabilizer allow for a greater variety of conductor cross-section designs and stabilizer compositions.

Diffusion Barriers. Good fabrication practice results in an excellent metallurgical bond between the composite components by the stage of the process at which precipitation heat treatments are applied. At α-Ti, precipitation temperatures Cu and Ti at an Nb–Ti/Cu interface will react to form hard intermetallic Ti–Cu (most commonly $TiCu_4$) compounds (25, 26). The hard intermetallics do not codeform with the filaments and will agglomerate as final wire drawing proceeds. The agglomeration of hard particles results in filament nonuniform filament cross sections and ultimately can lead to strand failure. The practice of applying Nb diffusion barriers between the Nb–Ti and the stabilizer to improve filament uniformity and strand predates the acute intermetallic problems caused by aggressive multiple precipitation heat treatments (27). Nb diffusion barriers became commonplace after it was clear that they would be required to achieve the high critical current densities required by the superconducting supercollider project (28). Nb is effective at inhibiting the formation of the Ti–Cu intermetallics and is mechanically compatible with the Nb–Ti alloy rod.

The Nb barrier is normally applied as a sheet wrapped around the Nb–Ti rod before inserting into the stabilizer material. Because the Nb sheet does not contribute to the critical current density, the stability reduces the overall superconductor cross section and is kept to a minimum. The Nb sheet is not impervious to Cu or Ti diffusion and must be kept to a sufficient thickness so that Cu levels in the Nb–Ti do not reach high enough levels during heat treatment that $TiCu_4$ is formed. As the composite is deformed to smaller and smaller cross section, so is the thickness of the diffusion barrier, thus the most critical processing stage for the Nb diffusion barrier is the final heat precipitation heat treatment. At this stage, not only is the barrier at its thinnest during heat treatment, but earlier heat treatments have produced Ti-rich α-Ti precipitates, some of which will be adjacent to the barrier. Although Cu and Nb have a very low mutual solubility, the high density of Nb and Nb–Ti grain boundaries in the cold-worked composites provides sufficient pathways for Cu diffusion. Faase et al. (29) have calculated that for an aggressive final heat treatment of 80 h at 420°C a minimum barrier thickness of 0.6 μm is required to prevent reaction layers in the filament (there is no significant reaction in the Cu for Cu-stabilized composites). For smaller filaments, this can represent a significant proportion of the nonstabilizer area.

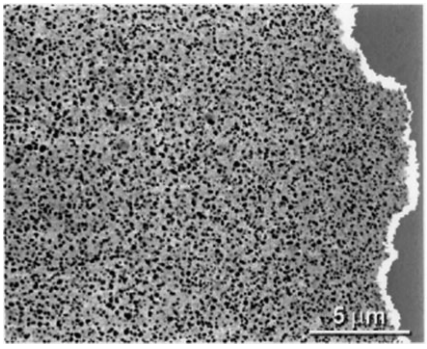

Figure 5. High-resolution back-scattered electron scanning electron microscope image of the Nb–Ti adjacent to an Nb diffusion barrier (white) after final precipitation heat treatment. Nonuniformity of the barrier is shown along with a zone of reduced precipitate (black) next to the barrier.

For instance, for a 6 μm final filament diameter design, a 0.6 μm barrier at final heat treatment size represents 4% of lost superconductor area. For a 2.5 μm final filament diameter the same thickness diffusion barrier represents a lost superconductor area of over 9%. The calculated predictions of required Nb thickness agree well the development of 6 μm filament strands for the superconducting supercollider where it was shown that 4 area % Nb barriers were required as opposed to 2 area % barriers used in early prototypes (30). Faase et al. also observed that the α-Ti precipitates adjacent to the Nb barrier were much smaller than elsewhere in the Nb–Ti. In addition to the formation of brittle intermetallics, Moreland et al. (31) found that Cu concentrations of $<3\%$ in the Nb–Ti significantly degraded the local energy gap. Reducing the temperature of the final precipitation heat treatment significantly reduces the required minimum barrier thickness but must be balanced against a reduced rate of precipitation. Figure 5 shows a transverse cross section of Nb–Ti filament adjacent to a Nb barrier after it has received the third of three precipitation heat treatments. The nonuniformity of the barrier thickness is clear in Fig. 5 as is a zone of reduced precipitate size adjacent to the barrier.

The grains of the BCC Nb barrier and the Nb–Ti superconductor deform under plane strain conditions such that their ⟨100⟩ directions align with the wire-drawing axis, and they thin in their ⟨001⟩ direction. Maintaining grain boundary continuity requires that both the Nb–Ti and Nb grains must intercurl around their neighbors during cold work (see Ref. 32). At the Nb–Ti/Nb interface the Nb grains intercurl with the Nb–Ti grains resulting in an uneven barrier thickness. As the grain size increases, the scale of Nb–Ti penetration into the barrier increases. Hessner et al. (33) showed that there was a linear relationship between increasing Nb–Ti grain size and increasing variation in Nb barrier thickness, providing an additional incentive to use fine-grained Nb–Ti alloy.

Strand Geometry and Filament Spacing. A wide variety of strand geometries are manufactured from Nb–Ti, ranging from large single-filament conductors to multifilamentary strands with more than 40,000 filaments. The low-

resistivity stabilizer tends to be much softer than the Nb–Ti superconductor, so attention has to be paid to producing a composite that is mechanically stable over the large extrusion and drawing reductions. Gregory et al. (34) established that the optimum mechanical stability for Nb–Ti/Cu multifilamentary composites was for a filament spacing-to-diameter *(s/d)* ratio of 0.15 (ratios of 0.15 to 0.20 are now typical). This ratio fixes the local stabilizer-to-superconductor ratio; and if additional stabilizer is required, it can be designed outside the filament pack. Ghosh et al. (35) established that for direct-current (*dc*) magnet application a minimum Cu thickness of 0.4 μm to 0.5 μm was required to reduce the magnetization associated with proximity filament coupling. For *s/d* ratios of 0.15 to 0.20, the minimum Cu thickness requirement limits the minimum filament diameter to 2.7 μm to 3.3 μm when using a pure Cu matrix. If smaller filaments are required, Ni or Mn can be added to the Cu between the filaments as explained earlier.

Composite Assembly. In its simplest form, an Nb–Ti rod with or without a barrier wrap is coextruded inside a high-purity Cu fine-grained can. The warm extrusion produces a well-bonded monofilament. For a multifilamentary application the monofilament composite can be drawn to an intermediate size so that it can be restacked in another Cu can (typically 250 mm to 360 mm in diameter and shaped to fit the extrusion chamber) to form a second extrusion composite. The monofilaments for restacking are usually drawn through a final hexagonal die to facilitate uniform strand packing. In addition to the Nb–Ti/Cu subelements the stack will also contain shaped Cu spacers and Cu hexes to fill voids and provide additional stabilizer if necessary. Some composite designs utilize a central Cu core (usually assembled from hexagonal Cu rods) which is thought to reduce center burst during extrusion (superconducting supercollider specifications required a Cu core). The composite must be densely packed to avoid upset during extrusion. Even after packing with Cu shims, some void space is inevitable in any multifilamentary stack. Normally the amount of void space in a well-packed composite is not sufficient to cause problems during extrusion; but in some cases particularly, when there are large numbers of small filaments, the extrusion billet may have to be isostatically compacted prior to extrusion. Single stacks of more than 22,000 filaments have been successfully fabricated. Alternatively, composites with 200 or fewer filaments can be fabricated by inserting bare Nb–Ti rods into holes in a stabilizer billet prepared by gun-drilling (see Ref. 36 for more examples). A good metallurgical bond is required between the composite components if uniform filament diameters and high yield are to be achieved, and this requires that contamination of the surfaces be kept to a minimum. The mobility of oxygen in Cu at processing temperatures also means that surface oxides must be removed from the high-purity Cu in order to maintain low resistivity and good mechanical properties. When the monofilament is fabricated at large size (100 mm to 200 mm diameter), it benefits from a low surface-to-volume ratio for the components. The restacked monofilaments suffer from a relatively large surface-to-volume ratio that increases as the diameter of the stacked filaments decreases. The importance of reducing chemical and particulate contamination cannot be overemphasized. Long lengths of strand (typically 10 km or more) are desired for many applications, and small particulate pickup that significantly reduces yield by strand breakage can occur in even tightly controlled large-scale production (37).

After the billet is assembled, the filaments are sealed under vacuum by electron-beam (or sometimes tungsten inert gas) welding a Cu lid onto the billet.

Extrusion

After preheating to 500° to 650°C the extrusion billets are conventionally extruded at ratios of 10:1 to 20:1 and then water-quenched. Lower temperatures are favored because they maintain a greater degree of cold work in the Nb–Ti but they require greater forces. Low extrusion speeds avoid excessive heating of the Nb–Ti. Hydrostatic extrusion may also be used when available and has the advantages of lower-temperature operation, higher yields available from higher length-to-diameter ratios, and an ability to coextrude a wider variety of material combinations. After successful extrusion, the composite is a well-bonded composite of a suitable size (50 mm to 90 mm in diameter) for cold work to proceed.

Cold Work

Superconducting Nb–Ti strands are fabricated in a cold-worked condition that is far greater than any other metallurgical process, with the possible exception of piano wire. The object of the cold work is to produce the final nanometer scale dispersion of pinning center. Understanding the role and importance of this highly strained state in the production of Nb–Ti strands is the key to the conventional process. The amount of cold work in the Nb–Ti normally can be represented by the true strain, Ω_T, which is given by Eq. (1):

$$\epsilon_t = \ln A_0/A = 2\ln d_0/d \tag{1}$$

where d_0 and A_0 are the starting diameter and cross-sectional area of the alloy rod at the final recrystallization anneal, respectively, and d and A are the diameter and area of the Nb–Ti after cold work. Figure 6 illustrates the conventional process in terms of cold-work strain for a composite fabricated from a cold-worked rod and given three heat treatments. The total available cold-work strain available for processing the Nb–Ti is termed the "strain space" and is limited by the initial annealed Nb–Ti rod size and the final filament diameter. Warm extrusions increase the cold work in the Nb–Ti at a reduced rate compared with similar reductions performed by rod or wire drawing and consequently reduce the effective strain space. Increasing the temperature of extrusion improves the bonding between the composite components but reduces the available cold-work strain.

The strain space can be further subdivided into three regions, each requiring a minimum cold-work strain to be effective:

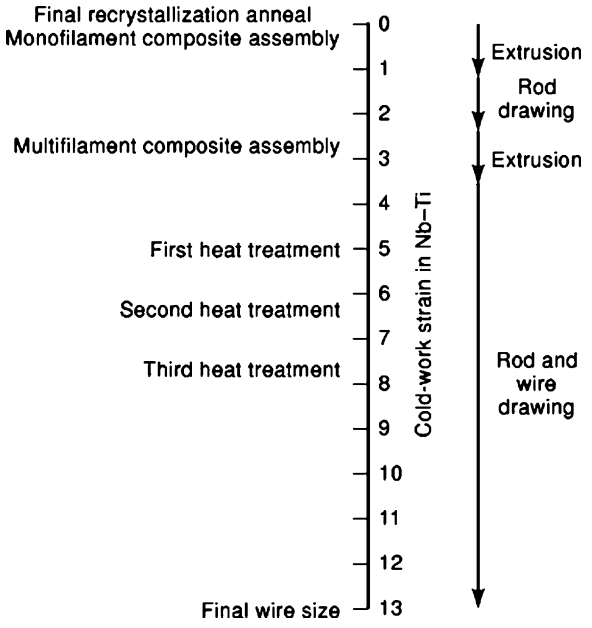

Figure 6. Schematic illustration of the conventional process for Nb–Ti superconductors in terms of cold-work strain.

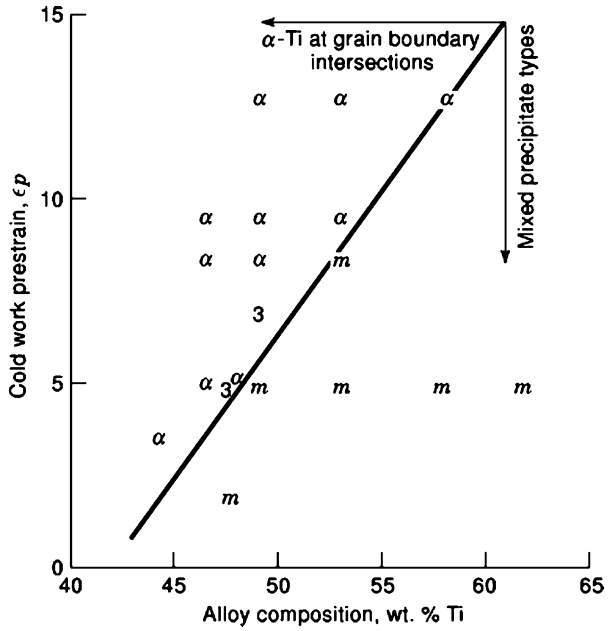

Figure 7. The morphology and location of precipitation in cold-worked Nb–Ti alloys are determined by the amount of cold work in the microstructure. As the Ti content is increased, the cold work required to produce optimum α-Ti (only at grain boundary intersections) increases. In this compilation of data (39–44), optimum precipitation is denoted by the symbol α, and mixed precipitate morphology is denoted by the letter m for heat treatment at 420°C. The number *3* identifies where mixed-mode precipitation has also been observed for 375°C heat treatments.

1. Prestrain, ε_p, the cold-work strain before the initial precipitation heat treatment.
2. The inter-heat treatment strain, $\Delta\varepsilon_{HT}$, the strain required between precipitation heat treatments.
3. The final strain, ε_f, the strain required to reduce the precipitate size to final optimum pinning size.

The cold work performs seven primary functions:

1. Encouraging the formation of the preferred precipitate phase and morphology.
2. Improving microchemical homogeneity by mechanical mixing both prior to heat treatment and after heat treatment when local Ti depletion has occurred.
3. Increasing the density of precipitate nucleation sites.
4. Increasing the grain boundary density, thereby increasing diffusion rates (grain boundary diffusion being considerably faster than bulk interdiffusion).
5. Reducing the average diffusion distance to the precipitate nucleation site.
6. Increasing the volume of precipitate by multiple strain/heat treatment cycles.
7. Reducing the precipitate dimensions from the precipitation scale of 100 nm to 300 nm diameter to the pinning scale of 1 nm to 5 nm.

The cold work is applied to the extruded composite by standard rod- and wire-drawing techniques. The rod or wire is pulled through a shaped die that uniformly reduces the cross-sectional area by 15% to 25%. As the strand becomes smaller in diameter, multiple die machines are used to apply more than area reduction in a single pass. The amount of cold work in a single-phase Nb–Ti alloy can be monitored using hardness testing: As the strain in the Nb–Ti increases, so does the hardness (38).

Buckett and Larbalestier (39) established that a minimum cold-work strain of approximately 5 was required before precipitation heat treatment to ensure the optimum precipitation mode, that of α-Ti precipitates located at grain boundary intersections. At lower strains, ω phase and/or intragranular Widmanstätten were formed, producing inhomogeneous microstructures that reduced workability. Lee et al. (40) systematically studied the relationship between prestrain, precipitate morphology, and alloy and showed a relationship between Nb–Ti composition and the required cold-work prestrain required to avoid strains ω phase and/or intragranular Widmanstätten α-Ti (40). Figure 7 illustrates the strong increase in required prestrain with increasing Ti content. This relationship is very important because it not only explains the importance of a homogeneous alloy composition but also explains the difficulties associated with processing high Ti alloys. An increase in ε_p of roughly 0.77 is required for each wt. % Ti increase in composition. Figure 8 shows the large amount of ω phase and or intragranular Widmanstätten α-Ti that can be produced by heat treating a high-Ti alloy (in this case, Nb–54 wt. % Ti) at too low a prestrain. By a true strain of 5 to 7 a high-angle grain structure of regular, small diameter (50 nm to 100 nm) grains has been produced by the large cold-work strain. Increasing the prestrain further homogenizes and refines the microstructure.

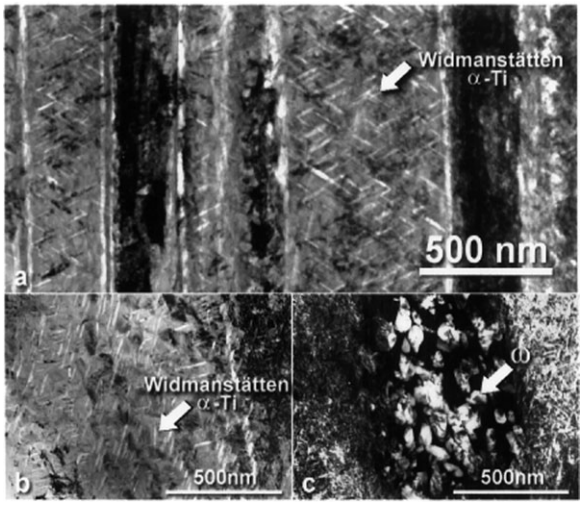

Figure 8. Transmission electron microscope image in bright field (a, b), and dark field using an omega reflection (c) of an Nb–54 wt. % Ti alloy after precipitation heat treatment. The heat treatment was applied at a cold-work prestrain of 5, which is insufficient to avoid the deleterious ω phase and or intragranular Widmanstätten α-Ti forms of precipitation. In (a) the microstructure is shown in longitudinal cross section with the drawing axis running down the page. Images (b) and (c) are of the same transverse cross-sectional area with the dark-field image bringing out contrast from the ω phase.

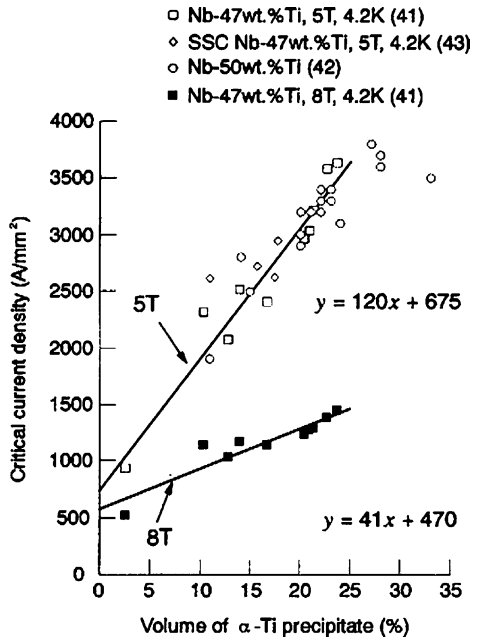

Figure 9. The peak critical current density increases linearly with volume percent of α-Ti precipitate over the range of 3% to 25 vol. % α-Ti for Nb–47 wt. % Ti (41, 43). Similar results have been shown for 50 wt. % Ti (42). Least squares fit dependencies for the Nb–47 wt. % Ti data are shown for applied fields of 5 T and 8 T.

Precipitation Heat Treatment

Lee et al. (41) first established a linear relationship between the optimized critical current density and the volume of precipitate in a laboratory-scale monofilamentary composite fabricated from Nb–47 wt. % Ti alloy as shown in Fig. 9. The relationship extended from 0% of the strand volume being precipitated (non-heat-treated) to 25 vol. %. Chernyj et al. (42) extended this relationship to an Nb–50 wt. % Ti alloy and a maximum volume percent of α-Ti of 28%. A wider study of strands produced by different manufacturers for the superconducting supercollider confirmed the linear relationship for industrial-scale strands (43). The importance of maximizing the amount of precipitate in the strand is unambiguous. Precipitate is produced in the Nb–Ti by heat treatments at 375° to 42°C for a duration of typically 40 h to 80 h. Increasing the temperature increases the precipitation rate but increases the precipitate diameter and the low-field J_c to high-field J_c ratio (43). The amount of precipitation is also dependent on the alloy composition; the quantity of α-Ti produced by the first precipitation heat treatment increases strongly with Ti content (44) as shown in Fig. 10. This relationship shows how too low a Ti content in the Nb–Ti alloy can result in insufficient precipitation for high critical current density and how a large local variation in Ti content can lead to an inhomogeneous distribution of precipitates and, subsequently, flux-pinning sites.

After approximately 10 vol. % precipitate has been produced in the first heat treatment, it becomes very difficult to produce significantly more without excessively long heat treatment times. By applying additional cold-work strain to the microstructure, more precipitate is produced

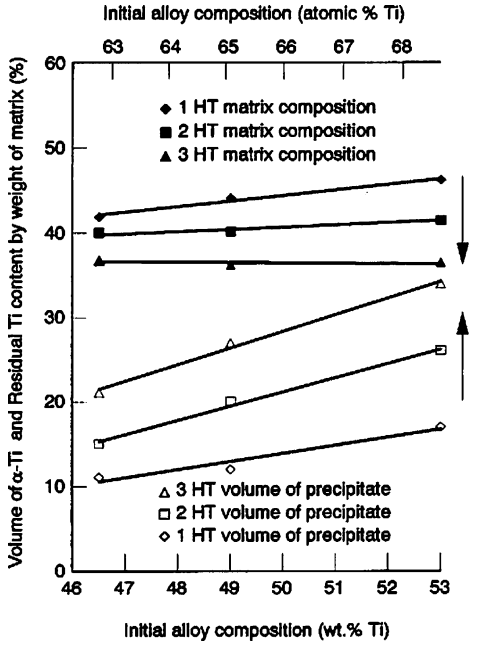

Figure 10. The precipitation rate in Nb–Ti increases strongly with Ti content in Nb–Ti alloys. Additional heat treatments further increase the amount of precipitate. As additional heat treatment and strain cycles are applied, and more precipitate is produced, the residual Ti content of the β-Nb–Ti matrix drops until insufficient Ti is left to drive further precipitation. In this graph, data from one and two heat treatments (40) are combined with data from three heat treatments of 80 h at 420°C. The average residual matrix composition is calculated assuming an α-Ti composition of Nb–3.75 at. % Ti.

(as shown in Fig. 10 for the second heat treatment). An optimum balance between increased precipitate volume and minimum strain space is at a strain of approximately 1.2 (12). Three or more heat-treatment and strain cycles are normally required to produce the 20 vol. % or more precipitate in the microstructure required for high critical current densities ($J_c > 3000$ A/mm^2 at 5 T and 4.2 K). As the α-Ti is precipitated, the composition of the β-Nb–Ti is depleted in Ti until it reaches between 36 wt. % Ti and 37 wt. % Ti, at which point there is insufficient Ti to drive further precipitation. More aggressive heat treatment is more likely to compromise the Nb diffusion barrier and coarsen the precipitate size.

After the final heat treatment the microstructure viewed transverse to the drawing axis consists of a uniform distribution of roughly equiaxed α-Ti precipitates, 80 nm to 200 nm in diameter, in a matrix of equiaxed Nb–Ti grains of similar dimensions. Viewed in longitudinal cross section the α-Ti and β-Nb–Ti grains are somewhat elongated along the drawing axis with an aspect ratio of 4 to 15 depending on the processing history. Further cold-work strain is required to reduce the dimensions of the precipitates so that they can pin flux efficiently. During the α-Ti precipitation heat treatments, the β-Nb–Ti matrix has been depleted in Ti to a level of 37 wt. % Ti to 38 wt. % Ti, and the H_{c2} and T_c of the composite at this point in processing are the same as the values of single-phase material of these lower Ti levels (5).

Final Wire Drawing

The plain strain-imposed intercurling of the Nb–Ti grains that is so deleterious to barrier uniformity also results in the distortion of the α-Ti precipitates into densely folded sheets during final wire drawing. The folding process rapidly decreases the precipitate thickness and spacing and with a dependence of $d^{1.6}$ (where d is the strand diameter) and increases the precipitate length per area with a dependence of $d^{-1.6}$ as measured by Meingast et al. (5). As the microstructure is refined toward optimum size the bulk pinning force increases and the peak in the bulk pinning force moves to higher field as shown in Fig. 11 (data from Ref. 45). The H_{c2} and the T_c gradually return to the values of the original single phase starting alloy as the precipitate are refined toward and below the superconducting coherence length, ξ (5). The critical current density increases as the microstructure is refined until it reaches a peak, after which there is a steady decline. The peak in J_c for a monofilament or a multifilamentary strand with uniform filaments occurs at a final strain of approximately 5. If the filaments are nonuniform in cross section (sausaged), the peak occurs earlier and at a lower critical current density. A strand that has a premature (and lowered) peak in J_c during final drawing is described as *extrinsically* limited because it has not attained the intrinsic critical current of the microstructure. The most common source of extrinsic limitation is sausaging of the filaments due to intermetallic formation or lack of bonding between the components of the composite. The degree to which a composite has been extrinsically limited can be observed by examining the sharpness of the resistive transition when measuring the critical current, I_c. Volker (46) showed that the shape of the transition curve near its onset can be approximated by

$$V \propto I^n \tag{2}$$

where V is the voltage across, I is the current in the superconductor, and n is the resistive transition index. For a nonextrinsically limited superconductor the value of n at 5 T, 4.2 K, can be 70 or higher. By quantifying the variation in filament cross-sectional area by image analysis, the amount of filament sausaging can be measured directly (47). A high critical current density superconductor with a high n-value is shown in Fig. 12. The strand is one of a number of high-performance wires developed for the superconducting supercollider (48). The filament sausaging in this strand has been reduced to a very low level (a coefficient of variation for the filament cross-sectional areas of approximately 2%). With tight quality control, uniform properties and piece lengths exceeding 10 km should be expected.

The specific pinning force for the α-Ti precipitates falls from 360 N/m^2 for an average sheet thickness of 2.6 nm, to 200 N/m^2 for a 1 nm average sheet thickness (14, 49) but this is more than compensated for by the increase in precipitate density caused by the continued folding of the α-Ti sheets.

Final Processing

Twisting. Just before a multifilamentary strand has reached final size, it is usually twisted about its drawing axis. The twisting is required to reduce flux-jump instability caused by varying external fields, reduce instabilities caused by self-field, and reduce eddy-current losses. The tightness of the required twist increases with the expected rate of change of field. The required twist pitch for a superconducting supercollider strand, a relatively steady-state magnet, was approximately 80 rotations along the drawing axis per meter, while for ac application with a similarly sized strand the number of twists per meter might be 300. The twisting occurs just before the strand is reduced to final size so that it can be locked in by a final drawing pass or by final shaping.

Final Shaping. The final shape of the strand cross section need not be round in cross section: It can also be shaped into square or rectangular cross section by the use of independently adjusted rollers operating along the strand surface.

Cabling. Individual strands can be cabled or braided together to form a conductor with a higher current-carrying capacity. The most common design for Nb–Ti magnets is the Rutherford cable, which consists of two parallel flat layers of strands. Using this approach, high-aspect-ratio cables can be produced with as many as 46 strands (50). As was the case for the individual filaments, the strands are transposed around the cable, forming a densely packed square or rectangular cross-section spiral. The design consideration for Superconducting Supercollider Laboratory cable are discussed in Ref. 51. The compaction of the strand around the squared cable edges severely distorts the strand

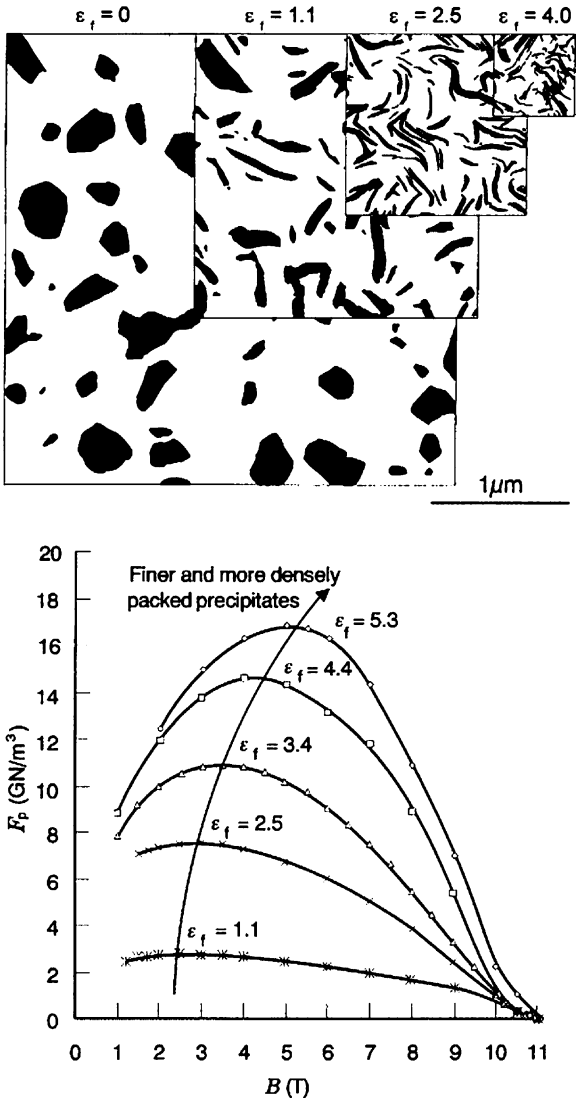

Figure 11. For conventionally processed Nb–Ti the bulk pinning force increases in magnitude with drawing strain after the last heat treatment. The increase occurs at all fields as the precipitate size and spacing are reduced to less than a coherence length in thickness (45). The refinement of the microstructure with increasing strain for the same strand is shown schematically in transverse cross-sections with the α-Ti precipitates in black.

cross section, but the excellent mechanical properties of Nb–Ti/Cu composites combined with good strand design and advances in cabling technology have reduced cabling degradation to minimal levels (52).

Nb–Ti–Ta

The addition of Ta to Nb–Ti alloys suppresses the paramagnetic limitation of H_{c2} by the large orbital moment of the alloys (53). Although Ta is only of benefit below 4.2 K (54), it has a relatively long history of study because it should extend the useful field range of ductile superconductors by 1 T or more (55). So far, however, improved H_{c2} has not translated effectively into improvements in J_c, except very near to H_{c2} (above 11 T). Lazarev et al. (56) were able to

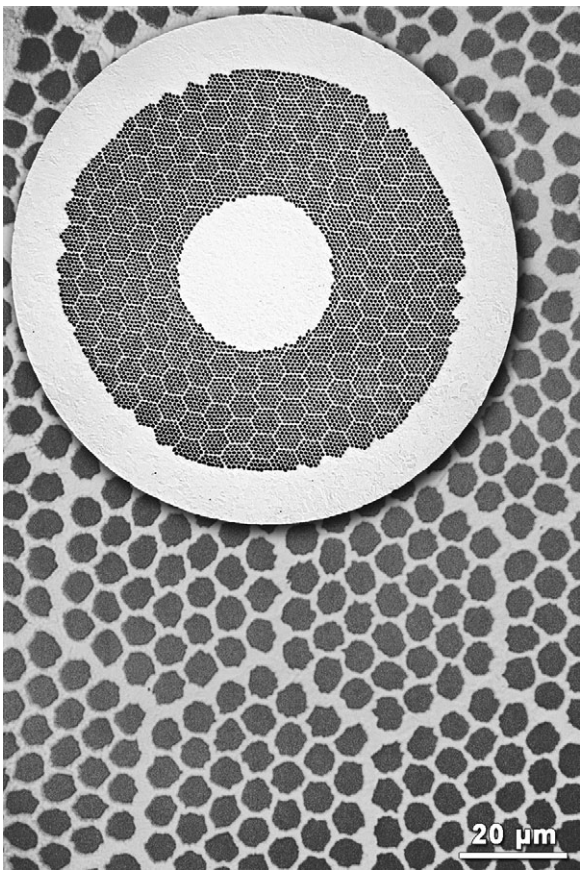

Figure 12. Partial cross-section of a strand designed for the Large Hadron Collider at CERN by IGC Advanced Superconductors (now Luvata Waterbury, Inc.). 250,000 km of Nb-Ti strand were required in order to produce magnets for the 27 kilometer LHC ring, including 1232 dipoles and 858 quadrupoles. Each dipole was 15 m in length and weighed 35 tonnes. The LHC uses 1.9 K operation to push the Nb-Ti based magnets beyond 8 T. Inset is the full strand cross-section showing the individual filament stacking units. Each LHC strand has 6425 or 8800 filaments of 6 or 7 μm diameter respectively.

attain a critical current density 1000 A/mm^2 at a field of 11.5 T (2.05 K) using an Nb–37 wt. % Ti–22 wt. % Ta alloy. Ta has an even higher melting point than Nb, making the fabrication of chemically homogeneous ternary alloys particularly difficult. The behavior of Nb–Ti–Ta alloys under the conventional process is similar to that of binary alloys, but the precipitates do not appear to pin as efficiently (57).

THE APC PROCESS

The quantity, composition, and distribution of pinning center as well as the composition of the matrix are limited, in the conventional process, by the thermodynamics of the Nb–Ti phase diagram. Additional precipitate can be produced by increasing Ti content of the alloy (as shown in Figure 10), but that is more than offset by the decrease in H_{c2} (Fig. 2). The result is a critical current limit in conventionally processed Nb–Ti superconductors of approximately 3800 A/mm^2, at 4.2 K and 5 T. An alternative ap-

proach is to fabricate the microstructure by mechanically assembling the desired components of the microstructure at large size and reducing the microstructure to the appropriate size by extrusion and cold drawing (58, 59). The engineered microstructural rods can be restacked into a composite just as for a conventional Nb–Ti superconductor, but no precipitation heat treatments are required. An intermediate approach developed by Supercon, Inc. (60) uses a low-temperature diffusion heat treatment to modify a densely packed microstructure fabricated from layer of pure Nb and Ti. The diffusion-modified APC has been successfully used in solenoid, model dipole (61), and MRI magnets (62). Round-wire APC superconductors and multilayers have developed zero-field J_c up to 10% of the theoretical upper limit provided by the depairing current density J_d. ($J_d \sim H_c/\lambda$) (e.g., Refs. 63 and 64), where λ is the penetration depth. APC superconductors fabricated with Nb pins perform particularly well at low fields (up to about 5 T to 7 T), and J_c values approaching 7500 A/mm^2 at 3 T (65, 66) have been achieved (25% of Nb pinning center in an Nb–47 wt. % Ti matrix). Nb has been a preferred pinning material because of its mechanical compatibility with the Nb–Ti matrix. Even using Nb, however, poor workability and increased costs associated with assembly and yield have so far limited the commercial application of APC composites. The components of an engineered microstructure must initially be large enough to be stacked by hand (or possibly machine); consequently the engineered pins must undergo a far greater deformation to reach optimum size than for α-Ti precipitates which start at 100 nm to 200 nm in diameter. The larger deformation and multiple extrusions and the restacks required by the APC process result in a microstructure that can be much less uniform than for the conventional process (67). For this reason, processes that can use smaller cross-sectional starting dimension, such as stacked or wrapped sheet, can result in superior properties such as the J_c of 4250 A/mm^2 at 5 T and 4.2 K, achieved by Matsumoto et al. (68) with stacked sheets of Nb–50 wt. % Ti and 28 vol. % of Nb sheets. Because of the large amount of cold work in the engineered microstructure, it is extremely sensitive to heating during extrusion; the highest round-wire J_c (5 T, 4.2 K) of 4600 A/mm^2 was achieved by Heussner et al. (69). For the Nb pins, similar volumes of pinning material are required as for conventionally processed materials; but by using ferromagnetic pins (Fe or Ni) the required pin volume to achieve high critical current density has been reduced to only 2 vol. % (70). Such developments suggest that there are still exciting advances that can be made in the development of ductile Nb–Ti-based superconductors.

2 K OPERATION

The relatively low T_c of Nb-Ti allows means that considerable gains in H_{c2} and and J_c can be gained from lowering the temperature of operation using superfluid liquid He, typically at 1.8 to 2 K. This has been recently exploited by the Large Hadron Collider project at CERN, which operates at 1.9 K so that the magnetic field can be pushed beyond 8 T (71). Boutboul et al. (72) have shown that the critical current density of production LHC strands, from five different sources, when measured at 1.9 K and 9 T (2275–2376 A/mm^2) is approximately that of the same strands at 4.2 K and only 6 T.

BIBLIOGRAPHY

1. E. W. Collings, *Applied Superconductivity, Metallurgy, and Physics of Titanium Alloys*, vol.**1**: *Fundamentals*, New York: Plenum, 1986.
2. E. W. Collings, *Applied Superconductivity, Metallurgy, and Physics of Titanium Alloys*, vol.**2**: *Applications*, New York: Plenum, 1986.
3. E. W. Collings, *A Sourcebook of Titanium Alloy Superconductivity*, New York: Plenum, 1983.
4. H. Muller, The upper critical field of niobium–titanium, PhD thesis, Univ. Wisconsin—Madison, 1990.
5. C. Meingast, P. J. Lee, D. C. Larbalestier, Quantitative description of a high J_c Nb–Ti superconductor during its final optimization strain. I. Microstructure,T_c, H_{c2} and resistivity, *J. Appl. Phys.*, **66**: 5962–5970, 1989.
6. D. L. Moffat, Phase transformations in the titanium–niobium binary alloy system, PhD thesis, Univ. Wisconsin—Madison, 1985.
7. I. Pfeiffer, H. Hillmann, Der Einfluss er Struktur auf die Supraleitungseigenschaften von NbTi50 und NbTi65, *Acta Metall.*, **16**: 1429–1439, 1968.
8. M. Hansen *et al.*, Systems titanium–molybdenum and titanium–columbium, *J. Metals*, **3**: 881–888, 1951.
9. L. Kaufman, H. Bernstein, *Computer Calculations of Phase Diagrams*, New York: Academic Press, 1970.
10. D. L. Moffat, U. R. Kattner, The stable and metastable Ti–Nb phase diagram, *Metall. Trans.*, **19A**: 2389–2397, 1988.
11. D. L. Moffat, D. C. Larbalestier, The competition between martensite and omega in quenched Ti–Nb alloys, *Metall. Trans.*, **19A**: 1677–1686, 1988.
12. Li Chengren, D. C. Larbalestier, Development of high critical current densities in niobium 46.5 wt % titanium, *Cryogenics*, **27**: 171–177, 1987.
13. D. C. Larbalestier, A. W. West, New perspectives on flux pinning in niobium–titanium composite superconductors, *Acta Metall.*, **32**: 1871–1881, 1984.
14. P. J. Lee, D. C. Larbalestier, Development of nanometer scale structures in composites of Nb–Ti and their effect on the superconducting critical current density, *Acta Metall.*, **35**: 2526–2536, 1987.
15. D. C. Larbalestier *et al.*, High critical current densities in industrial scale composites made from high homogeneity Nb46.5T, *IEEE Trans. Magn.*, **21**: 269–272, 1985.
16. Specification for Niobium Titanium Alloy for the Superconducting Supercollider, MSD Document Control, Dallas, Texas: Superconducting Supercollider Laboratory, 1992, SSC-Mag-M-4000A.
17. D. B. Smathers *et al.*, Improved niobium 47 weight % titanium composition by iron addition, *Mater. Trans., Jpn. Inst. Metals*, **37** (3): 519–526, 1996.
18. R. Schlatter, Electrical and magnetic interactions in vacuum-arc remelting and their effect on the metallurgical quality of speciality steels, *J. Vac. Sci. Technol.*, **11** (6): 1047–1054, 1974.

19. H. Hillmann, Fabricaton technology of superconducting material, in S. Foner and B. B. Schwartz (eds.), *Superconducting Materials Science*, New York: Plenum, 1981, p. 275.
20. I. Hlasnik *et al.*, Properties of superconducting NbTi superfine filament composites with diameter ≤ 0.1 μm, *Cryogenics*, **25** (10): 558–564, 1985.
21. J. R. Cave *et al.*, Reduction of AC loss in ultra-fine multifilamentary NbTi wires, *IEEE Trans. Magn.*, **25** (2): 1945–1948, 1989.
22. T. S. Kreilick *et al.*, Reduction of coupling in fine filamentary Cu/NbTi composites by the addition of manganese to the matrix, *Adv. Cryog. Eng.*, **34**: 895–900, 1988.
23. M. K. Rudziak, T. Wong, J. Wong, Development of APC NbTi superconductors with internal high purity aluminum stabilizer, *IEEE Trans. Appl. Supercond.*, **7**: 1197–1200, 1997.
24. H. C. Kanithi, D. Phillips, B. A. Zeitlin, Further development of aluminum clad superconductors, *IEEE Trans. Magn.*, **27**: 1803–1806, 1991.
25. D. C. Larbalestier *et al.*, High critical current densities in fine filament NbTi superconductors, *IEEE Trans. Nucl. Sci.*, **32**: 3743–3745, 1985.
26. M. Garber *et al.*, Effect of Cu_4Ti compound formation on the characteristics of NbTi accelerator magnet wire, *IEEE Trans. Nucl. Sci.*, **32**: 3681–3683, 1985.
27. E. Gregory, in R. W. Meyerhoff (ed.), *Manufacture of Superconducting Materials*, Metals Park, OH: Amer. Soc. Metals, 1977, pp. 1–16.
28. R. M. Scanlan, J. Royet, R. Hannaford, Evaluation of various fabrication techniques for fabrication of fine filament NbTi superconductors, *IEEE Trans. Magn.*, **23**: 1719–1723, 1987.
29. K. J. Faase *et al.*, Diffusional reaction rates through the Nb wrap in SSC and other advanced multifilamentary Nb–46.5 wt. %Ti composites. *Adv. Cryog. Eng.*, **38**: 723–730, 1992.
30. Y. High *et al.*, Quantitative analysis of sausaging in Nb barrier clad filaments of Nb–46.5 wt % Ti as a function of filament diameter and heat treatment, *Adv. Cryog. Eng. (Mater.)*, **38**: 647–652, 1992.
31. J. Moreland, J. W. Ekin, L. F. Goodrich, Electron tunneling into superconducting filaments: Depth profiling the energy gap of NbTi filaments from magnet wires, *Adv. Cryog. Eng. (Mater.)*, **32**: 1101–1108, 1986.
32. W. F. Hosford, Jr., Microstructural changes during deformation of [011] fiber textures metals, *Trans. Metall. Soc. AIME*, **230**: 12–15, 1964.
33. R. Heussner, P. Lee, D. Larbalestier, Non-uniform deformation of niobium diffusion barriers in niobium–titanium wire, *IEEE Trans. Appl. Supercond.*, **3**: 757–760, 1993.
34. E. Gregory *et al.*, Importance of spacing in the development of high current densities in multifilamentary superconductors, *Cryogenics*, **27**: 178, 1987.
35. A. K. Ghosh *et al.*, Anomalous low field magnetization in fine filament NbTi conductors, *IEEE Trans. Magn.*, **23**: 1724–1772, 1987.
36. T. S. Kreilick, Niobium–titanium superconductors, in *Metals Handbook*, 10th ed., vol. 2: *Properties and Selection: Nonferrous Alloys and Special-Purpose Materials*, ASM Int., 1990, pp. 1043–1057.
37. P. Valaris *et al.*, A statistical evaluation of recent SSC conductors produced at IGC/ASI, *IEEE Trans. Magn.*, **27**: 1752–1754, 1991.
38. J. Parrell, P. Lee, D. Larbalestier, Cold work loss during heat treatment and extrusion of Nb–46.5 wt % Ti composites as measured by microhardness, *IEEE Trans. Appl. Supercond.*, **3**: 734–737, 1993.
39. M I. Buckett, D. C. Larbalestier, Precipitation at low strains in Nb%46.5 wt % Ti, *IEEE Trans. Magn.*, **23**: 1638–1641, 1987.
40. P. J. Lee, J. C. McKinell, D. C. Larbalestier, Microstructure control in high Ti–NbTi alloys, *IEEE Trans. Magn.*, **MAG-725**: 1918–1924, 1989.
41. P. J. Lee, J. C. McKinnell, D. C. Larbalestier, Restricted novel heat treatments for obtaining high J_c in Nb–46.5 wt % Ti, *Adv. Cryog. Eng. (Mater.)*, **36**: 287–294, 1990.
42. O. V. Chernyj *et al.*, Nb–Ti superconductors of a high current-carrying capacity, *Supercond. Sci. Technol.*, **4**: 318–323, 1991.
43. P. J. Lee, D. C. Larbalestier, An examination of the properties of SSC Phase II R&D strands, *IEEE Trans. Appl. Supercond.*, **3**: 833–841, 1993.
44. P. J. Lee, J. C. McKinell, D. C. Larbalestier, Progress in the understanding and manipulation in high J_c Nb–Ti alloy composites, in Y. Murakami (ed.), *Proc. of New Developments in Appl. Supercond.*, Singapore: World Scientific, 1989, pp. 357–362.
45. C. Meingast, D. C. Larbalestier, Quantitative description of a very high critical current density Nb–Ti superconductor during its final optimization strain. II. Flux pinning mechanisms, *J. Appl. Phys.*, **66**: 5971–5983, 1989.
46. F. Voelker, Resistance in small, twisted, multicore superconducting wires, *Particle-Accelerators*, **1** (3): 205–207, 1970.
47. Y. High *et al.*, Quantitative analysis of sausaging in Nb barrier clad filaments of Nb–46.5 wt % Ti as a function of filament diameter and heat treatment, *Adv. Cryog. Eng. (Mater.)*, **38**: 647–652, 1992.
48. P. Valaris *et al.*, SSCL phase 1 inner cable development program at IGC Advanced Superconductors, Inc., *IEEE Trans. Appl. Supercond.*, **3**: 705–708, 1993.
49. P. J. Lee, D. C. Larbalestier, Determination of the flux pinning force of α-Ti ribbons in Nb–46.5 wt. % Ti produced by heat treatments of varying temperature, duration and frequency, *J. Mater. Sci.*, **23**: 3951–3957, 1988.
50. R. Scanlan *et al.*, Design and fabrication of a high aspect ratio cable for a high gradient quadrupole magnet, *IEEE Trans. Appl. Supercond.*, **7**: 936–938, 1997.
51. D. Christopherson *et al.*, SSC 40 mm cable results and 50 mm design discussions, *IEEE Trans. Magn.*, **27**: 1881–1883, 1991.
52. M. Garber *et al.*, Superconducting wire and cable for RHIC, *IEEE Trans. Magn.*, **30**: 1722–1725, 1994.
53. M. Suenaga, K. M. Ralls, Some superconducting properties of Ti–Nb–Ta ternary alloys, *J. Appl. Phys.*, **40**: 4457–4463, 1971.
54. D. G. Hawksworth, D. C. Larbalestier, Enhanced values of H_{c2} in Nb–Ti ternary and quaternary alloys, *Adv. Cryog. Eng.*, **26**: 479–486, 1980.
55. H. R. Segal *et al.*, NbTi based conductors for use in 12 Tesla toroidal field coils, *Proc. 8th Symp. Eng. Problems Fusion Res.*, New York: IEEE Press, 1980, pp. 255–259.
56. B. G. Lazarev *et al.*, The study of the microstructure and J_c in Nb–37Ti–22Ta superconductor produced with different duration of treatments, in H. W. Weber (ed.), *Proc. 7th Int. Workshop Critical Currents Supercond.*, Alpbach, Austria, Singapore: World Scientific, 1994, pp. 601–604.
57. P. J. Lee *et al.*, Microstructure property relationships in Nb–Ti–Ta, *IEEE Trans. Appl. Supercond.*, **3**: 1354–1357, 1993.
58. G. L. Dorofejev, E. Yu Klimenko, S. V. Frolov, Current carrying capacity of superconductors with artificial pinning centers, in C. Marinucci and P. Weymuth (eds.), *Proc. 9th Int. Conf.*

Magnet Technol., Villigen, Switzerland: Swiss Institute Nuclear Res., 1985, pp. 564–566.

59. B. A. Zeitlin, M. S. Walker, L. R. Motowidlo,Superconductors having controlled laminar pinning centers, and method of manufacturing same,US Patent 4,803,310, 1989.
60. M. K. Rudziak *et al.*, Development of APC Nb–Ti composite conductors at Supercon, Inc., *IEEE Trans. Appl. Supercond.*, **5**: 1709–1712, 1995.
61. R. M. Scanlan *et al.*, *IEEE Trans. Magn.*, **30**: 1627–1632, 1994.
62. C. Renaud *et al.*, First commercial application of NbTi superconductor employing artificial pinning centers, *IEEE Trans. Appl. Supercond.*, **5**: 1189–1192, 1995.
63. G. Stejic *et al.*, Effect of geometry on the critical currents of thin films, *Phys. Rev.*, **B49**: 1274–1288, 1994.
64. E. Kadyrov, A. Gurevich, D. C. Larbalestier, High critical current densities in Nb47%Ti multilayers with planar copper flux pinning nanostructure, *Appl. Phys. Lett.*, **68**: 1567–1569, 1996.
65. L. R. Motowidlo *et al.*, Multifilament NbTi with artificial pinning centers: The effect of alloy and pin material on the superconducting properties, *Appl. Phys. Lett.*, **61** (8): 991–993, 1992.
66. H. C. Kanithi *et al.*, Further developments in NbTi superconductors with Artificial Pinning Centers, *Adv. Cryog. Eng. (Mater.)*, **38**: 675–683, 1992.
67. P. J. Lee, D. C. Larbalestier, P. D. Jablonski, Quantificaton of pinning center thickness in conventionally processed and powder processed artificial pinning center microstructures, *IEEE Trans. Appl. Supercond.*, **5**: 1701–1704, 1995.
68. K. Matsumoto *et al.*, Enhanced J_c properties in superconducting NbTi composites by introducing Nb artificial pins with a layered structure, *Appl. Phys. Lett.*, **64** (1): 115–117, 1994.
69. R. W. Heussner *et al.*, Increased critical current density in Nb–Ti wires having Nb artificial pinning centers, *Appl. Phys. Lett.*, **70** (7): 901–903, 1997.
70. N. D. Rizzo *et al.*, Ferromagnetic artificial pinning centers in superconducting $Nb_{0.36}/Ti_{0.64}$ wires, *Appl. Phys. Lett.*, **69** (15): 2285–2287, 1996.
71. L. Rossi," Superconducting magnets for the LHC main lattice." *IEEE Trans. Appl. Supercond* **14.2**: 153–158, 2004.
72. T. Boutboul, S. Le Naour, D. Leroy, L. Oberli, V. Previtali," Critical current density in SC Nb-Ti strands in the 100 mT to 11 T applied field range", *IEEE Trans. Appl. Supercond.*, **16.2**: 1184–1187, 2006.

PETER J. LEE
University of
Wisconsin—Madison,
Madison, WI